Obtaining molecular orientation from second harmonic and sum frequency scattering experiments in water: Angular distribution and polarization dependence

Alex G. F. de Beer[a] and Sylvie Roke[a]
Max Planck Institute for Metals Research, Heisenbergstrasse 3, D70569 Stuttgart, Germany

(Received 3 February 2010; accepted 23 April 2010; published online 15 June 2010)

We present a method for determining molecular orientation from second-order nonlinear light scattering experiments. Our modeling shows that there is an optimal angular region, for which the scattering pattern is most sensitive to molecular orientation. We show that molecular orientation can be retrieved from measuring intensities at different polarization combinations, measuring the relative amplitudes of different vibrational modes of the same moiety and by analyzing the shape of the angular scattering pattern. We further show that for C_{2v} and C_{3v} point groups, the asymmetric stretch mode displays a higher sensitivity to molecular orientation than the corresponding symmetric mode. We have implemented the model in an interactive simulation program that may be found at http://www.mf.mpg.de/en/abteilungen/roke/simulation.html. © *2010 American Institute of Physics*. [doi:10.1063/1.3429969]

I. INTRODUCTION

Second harmonic generation (SHG) and sum frequency generation (SFG) are noninvasive techniques that can be applied *in situ* to investigate structural and dynamical properties of interfaces.[1,2] One particular interesting aspect of SHG and SFG is the possibility to retrieve the orientational distribution of molecular groups from polarization dependent measurements.[3]

In such a measurement a pair of visible [$\mathbf{E}(\omega_1)$, with wave vector $\mathbf{k}_1$] and infrared [$\mathbf{E}(\omega_2)$, with wave vector $\mathbf{k}_2$] beams, or a single visible beam [$\omega_1=\omega_2$ and $\mathbf{E}(\omega_1)=\mathbf{E}(\omega_2)$], is reflected from an interface. Different polarization combinations excite different components of the second-order surface susceptibility ($\boldsymbol{\chi}^{(2)}$), creating a second-order polarization of the form

$$P^{(2)}(\omega_0)_{0,i}=\chi^{(2)}_{ijk}(\omega_0=\omega_1+\omega_2)E(\omega_1)_{1,j}E(\omega_2)_{2,k}, \tag{1}$$

which is essentially an oscillating charge distribution. This polarization is the source of the emitted sum frequency field, whose intensity can be measured. The measured intensity is reflected in the direction of transverse momentum conservation (i.e., $k_{\|1}+k_{\|2}=k_{\|0}$) and takes the following form:

$$I(\omega_0)\propto|\mathbf{P}^{(2)}(\omega_0)_0|^2. \tag{2}$$

The second-order susceptibility can often be considered as arising solely from the surface molecules, and is therefore an orientation-weighed sum of the hyperpolarizability tensor ($\boldsymbol{\beta}^{(2)}$) of the surface molecules. $\beta^{(2)}_{abc}$ is the transition matrix element of the combined transitions, induced by the local electric field. The value of $\boldsymbol{\beta}^{(2)}$ is determined by the type of transition and the local molecular symmetry. For SHG this is typically the symmetry of the dominant electronic transition,[4–6] and for SFG this can be, for instance, the vibrational (anti-)symmetric stretch mode of a CH_3 or SO_3^- group with C_{3v} symmetry,[3,7–9] the stretch mode of a dangling O–H group with C_∞ symmetry,[10] or more extended excitations in an alpha helix or a beta sheet.[11,12] Every molecular group, therefore, has a distinct coordinate frame (a,b,c) relative to its symmetry axis, for which $\boldsymbol{\beta}^{(2)}$ has a limited number of nonvanishing components. It is possible to determine the orientation of such a molecular group relative to an interface by relating the local molecular coordinate system (a,b,c) spun up by the symmetry of the excitation to the surface coordinate system (i,j,k) via the following set of equations:[3,13]

$$\chi^{(2)}_{ijk}=N_s\langle T_{ia}T_{jb}T_{kc}\rangle\beta^{(2)}_{abc}, \tag{3}$$

where N_s is the number density of contributing molecules and $\langle T_{ia}T_{jb}T_{kc}\rangle$ is the average transformation from the molecular coordinate frame (a,b,c) to the surface coordinate frame (i,j,k). The transformation from $\boldsymbol{\beta}^{(2)}$ to $\boldsymbol{\chi}^{(2)}$ consists of a rotation around the molecular (group) axis, a tilt by an angle ϕ, and finally a rotation around the interface normal. For most interfaces it is reasonable to assume a rotational isotropy for the first and last rotation so that the $\boldsymbol{\chi}^{(2)}$ components only depend on the tilt angle of the molecule with respect to the surface normal (ϕ).[14]

Colloidal soft matter systems such as vesicles, polymer beads, emulsions, granular materials, and protein crystals dispersed in liquid or solid media have a particularly high surface-to-volume ratio. Consequently, the properties of these systems are mainly determined by their interfacial regions. Since it was demonstrated successfully by the Eisenthal group that second harmonic photons could be generated from the surface of colloidal particles[15] it has become possible to probe structure, charge,[16] and chemical changes[17,18] that occur at the surface of colloidal particles with electronically resonant or nonresonant second harmonic scattering (SHS)[19–28] and vibrationally resonant sum fre-

[a]Electronic mail: debeer@mf.mpg.de; roke@mf.mpg.de.

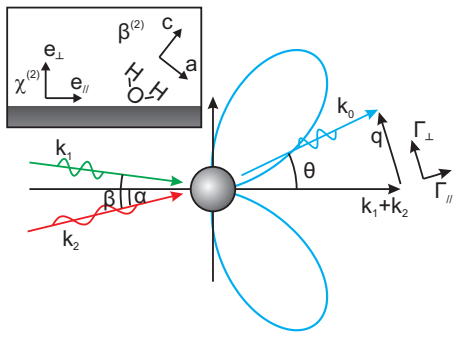

FIG. 1. Sketch (top view) of a scattering experiment. A spherical particle is illuminated with two pulses of different frequencies and wave vectors $\mathbf{k}_1$ and $\mathbf{k}_2$. A scattering pattern is generated at the sum of the two frequencies, which at an angle θ has wave vector $\mathbf{k}_0$. The scattering vector $\mathbf{q}$ is given as the difference $\mathbf{k}_0-\mathbf{k}_1-\mathbf{k}_2$ and forms the normal vector of the (imaginary) plane relative to which $\mathbf{\Gamma}^{(2)}$ is defined. Here we show the perpendicular $\Gamma_\perp$ and parallel $\Gamma_\parallel$ directions to that plane. The opening angle between the incoming laser pulses is β. The inset top left shows a close-up of the particle surface, relative to which the $\boldsymbol{\chi}^{(2)}$ components are defined. Shown are the parallel $\mathbf{e}_\parallel$ and perpendicular $\mathbf{e}_\perp$ directions. The values of the $\boldsymbol{\chi}^{(2)}$ components depend on the type, number, and orientation of molecules at the interface. For a water molecule, the principal coordinate axes are (a,b,c). The molecular hyperpolarizability $\boldsymbol{\beta}^{(2)}$ is defined relative to this coordinate system.

quency scattering (SFS).[29–34] These experiments were supported by a considerable amount of theoretical investigation, which allowed for a better understanding of the more complicated formalism that underlies[35–42] the scattering experiments. So far, little attention has been paid to how the molecular orientation with respect to the local surface normal (i.e., the radial direction in the case of a spherical particle) can be determined.

Here, we demonstrate how molecular orientation can be retrieved from SHS and SFS experiments. We simulate orientation-dependent angular scattering patterns for two commonly studied moieties, water and the methylene (CH_3) head group, representing C_{2v} and C_{3v} symmetries, respectively. We discuss how different molecular orientational distributions affect the scattering patterns, and how these patterns can be used to extract the molecular orientation. Our modeling shows that there is a certain angular region in the scattering pattern that is particularly sensitive to molecular orientation. Finally, the amplitude ratio between different vibrational modes of the same molecular group provides additional information, which may be used to improve accuracy.

II. THEORETICAL BACKGROUND FOR SHS AND SFS

A. Scattering formalism

In a SHS or SFS experiment the electromagnetic fields are overlapped in a dispersion. Figure 1 shows an overview of such an experiment: The two electric fields are incident on a spherical particle (e.g., a colloidal particle or an oil droplet in water) with radius R at the origin. At the interface of the particle a second-order polarization as that of Eq. (1) can be created. Because the particle size is in the order of the size range of the wavelength of the incoming beams, the generated second harmonic or sum frequency photons are scattered in a large angular distribution rather than reflected at a certain angle. The scattering angle can be measured with respect to the sum of the wave vectors $\mathbf{k}_0^0=\mathbf{k}_1+\mathbf{k}_2$. Scattered light is detected at an angle θ. The difference between the wave vector of the scattered light $\mathbf{k}_0$ and the forward direction defines a scattering vector $\mathbf{q}=\mathbf{k}_0-\mathbf{k}_0^0$. The opening angle between $\mathbf{k}_1$ and $\mathbf{k}_2$ is β, and the angle between $\mathbf{k}_0^0$ and $\mathbf{k}_2$ is α. Since SHS typically involves degenerate source fields, $\mathbf{k}_1$ and $\mathbf{k}_2$ are identical and the opening angle β is 0. Throughout this article, we assume spherical scatterers with an index of refraction that closely resembles that of the solvent [Rayleigh–Gans–Debye (RGD) approximation[29,35]]. Light polarization directions are defined relative to the plane in which $\mathbf{k}_1$ and $\mathbf{k}_2$ lie: Direction p(s) define a parallel (perpendicular) polarization relative to this plane.

The coordinate system (i,j,k) of the $\boldsymbol{\chi}^{(2)}$ tensor follows the local curvature of the particle interface [indicated by $\mathbf{e}_{\perp(\parallel)}$ for the perpendicular (tangential) directions with respect to the interface] and $\mathbf{E}_1$ and $\mathbf{E}_2$ have different phases on different parts of the interface. The nonlinear surface polarization therefore varies along the interface in strength, direction, and phase. The resulting polarization distribution leads to a scattering pattern in the far field. It is convenient to introduce an effective nonlinear susceptibility $\mathbf{\Gamma}^{(2)}$, which represents the nonlinear response of the entire particle surface[37] so that the sum frequency field corresponds to

$$E_{0,i} \propto \Gamma^{(2)}_{ijk}:E_{1,j}E_{2,k}. \tag{4}$$

For spherical particles, explicit expression for the $\mathbf{\Gamma}^{(2)}$ components have been derived.[29,37,39,41] In the RGD approximation, the symmetry of the $\mathbf{\Gamma}^{(2)}$ tensor reflects that of the $\boldsymbol{\chi}^{(2)}$ tensor: the nonvanishing components of $\mathbf{\Gamma}^{(2)}$ are $\Gamma^{(2)}_{\perp\perp\perp}$, $\Gamma^{(2)}_{\parallel\parallel\perp}$, $\Gamma^{(2)}_{\parallel\perp\parallel}$, and $\Gamma^{(2)}_{\perp\parallel\parallel}$. For $\mathbf{\Gamma}^{(2)}$, however, the directions $\perp$ and $\parallel$ denote laboratory-frame directions that are perpendicular and parallel to the hypothetical plane of which $\mathbf{q}$ is the normal direction. Such a choice of coordinate system allows for an analytical evaluation of the scattering patterns.

For nonchiral interfacial molecules, the relation between $\boldsymbol{\chi}^{(2)}$ and $\mathbf{\Gamma}^{(2)}$ depends on two scattering form factor functions[29,33,37,39] $F_1(qR)$ and $F_2(qR)$, which take the norm of the scattering vector $q=\|\mathbf{q}\|$ and the particle radius R as arguments,

$$F_1(qR) = 2\pi i\left(\frac{\sin(qR)}{(qR)^2} - \frac{\cos(qR)}{qR}\right), \tag{5}$$

$$F_2(qR) = 4\pi i\left(3\frac{\sin(qR)}{(qR)^4} - 3\frac{\cos(qR)}{(qR)^3} - \frac{\sin(qR)}{(qR)^2}\right), \tag{6}$$

$$qR = 2\|\mathbf{k}_0^0\|R\,\sin\left(\frac{\theta}{2}\right). \tag{7}$$

With these scattering functions, the $\mathbf{\Gamma}^{(2)}$ components can be related to the $\boldsymbol{\chi}^{(2)}$ components by a matrix multiplication,

$$\begin{pmatrix}\Gamma_1\\ \Gamma_2\\ \Gamma_3\\ \Gamma_4\end{pmatrix}=\begin{pmatrix}2F_1-5F_2 & 0 & 0 & 0\\ F_2 & 2F_1 & 0 & 0\\ F_2 & 0 & 2F_1 & 0\\ F_2 & 0 & 0 & 2F_1\end{pmatrix}\begin{pmatrix}\chi_1\\ \chi_2\\ \chi_3\\ \chi_4\end{pmatrix}, \tag{8}$$

where $\Gamma_1=\Gamma^{(2)}_{\perp\perp\perp}-\Gamma^{(2)}_{\parallel\parallel\perp}-\Gamma^{(2)}_{\parallel\perp\parallel}-\Gamma^{(2)}_{\perp\parallel\parallel}$, $\Gamma_2=\Gamma^{(2)}_{\parallel\parallel\perp}$, $\Gamma_3=\Gamma^{(2)}_{\parallel\perp\parallel}$, and $\Gamma_4=\Gamma^{(2)}_{\perp\parallel\parallel}$ and $\chi_1=\chi^{(2)}_{\perp\perp\perp}-\chi^{(2)}_{\parallel\parallel\perp}-\chi^{(2)}_{\parallel\perp\parallel}-\chi^{(2)}_{\perp\parallel\parallel}$, $\chi_2=\chi^{(2)}_{\parallel\parallel\perp}$, $\chi_3=\chi^{(2)}_{\parallel\perp\parallel}$, and $\chi_4=\chi^{(2)}_{\perp\parallel\parallel}$. For $\boldsymbol{\chi}^{(2)}$ the indices $\perp$ and $\parallel$ denote directions perpendicular and parallel to the interface (see Fig. 1); for $\boldsymbol{\Gamma}^{(2)}$ they denote directions perpendicular and parallel to the plane for which $\mathbf{q}$ is the normal vector.

The expressions for the scattered electric field amplitudes are similar to those for experiments on planar interfaces,

$$E_{\mathrm{ppp}}=\cos\left(\frac{\theta}{2}\right)\cos\left(\frac{\theta}{2}-\alpha\right)\cos\left(\frac{\theta}{2}-\alpha+\beta\right)\Gamma_1+\cos(\theta-\alpha+\beta)E_{\mathrm{ssp}}+\cos(\theta-\alpha)E_{\mathrm{sps}}+\cos(\beta)E_{\mathrm{pss}}, \tag{9}$$

$$E_{\mathrm{ssp}}=\cos\left(\frac{\theta}{2}-\alpha\right)\Gamma_2, \tag{10}$$

$$E_{\mathrm{sps}}=\cos\left(\frac{\theta}{2}-\alpha+\beta\right)\Gamma_3, \tag{11}$$

$$E_{\mathrm{pss}}=\cos\left(\frac{\theta}{2}\right)\Gamma_4, \tag{12}$$

where the indices "p" and "s" denote electric field polarizations. These relations are similar to the expressions for SHG and SFG in reflection mode.[37] Because of the one to one relationship between $\boldsymbol{\Gamma}^{(2)}$ and $\boldsymbol{\chi}^{(2)}$, it is possible to retrieve the relative values of the $\boldsymbol{\Gamma}^{(2)}$ components in a way similar to that for extracting $\boldsymbol{\chi}^{(2)}$ components from experiments on planar interfaces.[13]

B. Relation between $\boldsymbol{\beta}^{(2)}$ and $\boldsymbol{\chi}^{(2)}$

According to Eq. (3), the value of $\boldsymbol{\chi}^{(2)}$ depends on that of $\boldsymbol{\beta}^{(2)}$ and the average result of the coordinate transform from the molecular frame to the surface frame. When we assume that this transform only depends on the tilt angle (ϕ), only four independent $\boldsymbol{\chi}^{(2)}$ elements remain.[43,44] These elements depend on $\boldsymbol{\beta}^{(2)}$ and can be written in a matrix form equivalent to Eq. (8) if we define $\beta_1=\beta^{(2)}_{ccc}-\beta_2-\beta_3-\beta_4$, $\beta_2=(\beta^{(2)}_{aac}+\beta^{(2)}_{bbc})/2$, $\beta_3=(\beta^{(2)}_{aca}+\beta^{(2)}_{bcb})/2$, and $\beta_4=(\beta^{(2)}_{caa}+\beta^{(2)}_{cbb})/2$,

$$\begin{pmatrix}\chi_1\\ \chi_2\\ \chi_3\\ \chi_4\end{pmatrix}=\frac{N_s\langle\cos\phi\rangle}{2}\begin{pmatrix}(5D-3) & 0 & 0 & 0\\ (1-D) & 2 & 0 & 0\\ (1-D) & 0 & 2 & 0\\ (1-D) & 0 & 0 & 2\end{pmatrix}\begin{pmatrix}\beta_1\\ \beta_2\\ \beta_3\\ \beta_4\end{pmatrix}. \tag{13}$$

Here, $\langle\cos\phi\rangle$ is the average cosine of the molecular tilt angle ϕ and D is the ratio $\langle\cos^3\phi\rangle/\langle\cos\phi\rangle$.

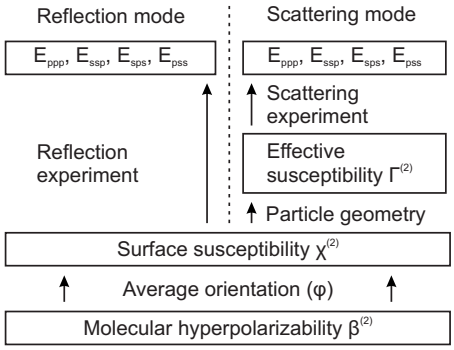

FIG. 2. Comparison of the determination of molecular orientation at achiral, isotropic surfaces from a nonlinear spectroscopy experiment. The left branch shows the procedure for experiment in a reflection setup, whereas the right branch shows the procedure for nonlinear light scattering. From the bottom up, every molecule at the interface has a hyperpolarizability $\boldsymbol{\beta}^{(2)}$, which contributes to the surface susceptibility $\boldsymbol{\chi}^{(2)}$ in a way that it is dependent on its orientation with respect to the surface. The average tilt angle ϕ determines the relative values of the components of $\boldsymbol{\chi}^{(2)}$. For a planar interface, these components can be measured directly using a reflection setup. In a suspension, however, the curved interface leads to an effective particle susceptibility tensor $\boldsymbol{\Gamma}^{(2)}$. The components of $\boldsymbol{\Gamma}^{(2)}$ can be treated analogous to a planar interface, with the exception that their values are dependent on the angle at which the signal is detected. Both for reflection and for scattering experiments, molecular orientations can be obtained by comparing the signal amplitudes of different light polarization combinations.

C. General relationships

With the above relations it is possible to evaluate molecular orientation from SHS and SFS experiments. Figure 2 shows a comparison between a reflection and a scattering experiment. The molecular hyperpolarizability $\boldsymbol{\beta}^{(2)}$ is coupled to the macroscopic surface susceptibility $\boldsymbol{\chi}^{(2)}$ by Eq. (13). The orientation parameter D determines the relative values of the $\boldsymbol{\chi}^{(2)}$ components. These surface susceptibility elements then determine the expression for the particle susceptibility $\boldsymbol{\Gamma}^{(2)}$, according to Eq. (8). This results in a scattering pattern that is determined by a linear combination of the functions F_1 and F_2 [Eq. (5)]. It is possible to probe the elements of $\boldsymbol{\Gamma}^{(2)}$ by measuring at different polarization combinations. Furthermore, the relative weights of F_1 and F_2 can be determined by measuring angular scattering intensity distributions. Thus, information on the orientation parameter D can be obtained.

Special cases arise when either β_1, χ_1, or Γ_1 is zero. In the first case, $\beta_1=0$, the nonlinear susceptibility becomes independent of D [see Eq. (13)], and therefore is only sensitive to $\langle\cos\phi\rangle$. Since the relative values of $\boldsymbol{\chi}^{(2)}$ do not change, a variation in $\langle\cos\phi\rangle$ will only modulate the overall intensity. The second case, $\chi_1=0$, occurs when $D=3/5$. This occurs at the "magic" orientation angle described by Simpson and Rowlen:[45] For a sufficiently broad distribution of molecular orientations, the value of D tends to 3/5. This effectively makes a broad distribution of molecules indistinguishable from a sharp distribution at an angle of $\phi=39.2°$. When $D=3/5$, the value of χ_1 vanishes so that in turn the elements of $\boldsymbol{\Gamma}^{(2)}$ depend only on F_1. Since F_1 has a node for $qR=4.49$, all scattered signal should vanish at this value for all polarizations. Finally, Γ_1 tends to zero when $2F_1-5F_2$ becomes small. This is the case at low values of qR. Since Γ_1 governs the differentiation between E_{ppp} and E_{ssp} [see Eq.

TABLE I. Relation between different $\boldsymbol{\beta}^{(2)}$ components for second harmonic and sum frequency processes. General rules hold for any molecule, while C_{2v} and C_{3v} rules hold for any molecule with the appropriate symmetry. Finally, rules for water/CH_2 hold only for the special geometry of these molecules, i.e., a relative angle between the stretching bonds of (close to) 104.5°.

	SHS	SFS (ss)	SFS (as)
General	$\beta_2=\beta_3$	$\beta_3\approx\beta_4$	$\beta_3\approx\beta_4$
C_{2v}/C_{3v}		$\beta_3=0$ $\beta_1=\beta_{ccc}^{(2)}-\beta_2$	$\beta_2=0$ $\beta_1=-2\beta_3$
Water/CH_2	$\beta_{ccc}^{(2)}\approx 0$ $\beta_1=-2\beta_2-\beta_4$	$\beta_2\approx\beta_{ccc}^{(2)}$ $\beta_1\approx 0$	

(9)], determining molecular orientation becomes more favorable at larger qR, and thus at larger scattering angles.

D. Second harmonic scattering

Relations between $\boldsymbol{\beta}^{(2)}$ components in a SHG process are governed by the symmetries of the dominant electronic transitions.[4,46] Table I summarizes some common relations between $\boldsymbol{\beta}^{(2)}$ components when certain molecular symmetries hold. In a second harmonic experiment, the source fields are degenerate, and therefore β_2 must be equal to β_3. For a C_{2v} symmetric molecule, the dominant electronic transition is typically a B-type transition.[47] For water, this means $\beta_{ccc}^{(2)}$ is negligible[6,48] so that $\beta_1=-2\beta_2-\beta_4$. Furthermore, Zhang and co-workers experimentally determined the ratio β_4/β_2 at 0.69 for water at a fundamental frequency of 800 nm.

E. Sum frequency scattering

In the case of a sum frequency process it is usually assumed that $\beta_3=\beta_4$ due to the symmetry of the Raman tensor far from resonance.[3,43,44] Two of the most common symmetry classes are C_{2v} and C_{3v}. For a C_{2v} symmetric molecule only seven components of $\boldsymbol{\beta}^{(2)}$ are nonzero: $\beta_{caa}^{(2)}$, $\beta_{cbb}^{(2)}$, $\beta_{aca}^{(2)}$, $\beta_{bcb}^{(2)}$, $\beta_{aac}^{(2)}$, $\beta_{bbc}^{(2)}$, and $\beta_{ccc}^{(2)}$, where c denotes the direction along the C_{2v} symmetry axis and (a,b) denote two mutually orthogonal directions perpendicular to the c-axis. The components of $\boldsymbol{\beta}^{(2)}$ separate into those of the asymmetric stretch (as) vibration (for which $\beta_1=-2\beta_3$ and $\beta_2=0$), and those of the symmetric stretch (ss) vibration (for which $\beta_3=\beta_4=0$). The same holds true for a C_{3v} symmetry, with the additional relations $\beta_{aac}^{(2)}=\beta_{bbc}^{(2)}$, $\beta_{aca}^{(2)}=\beta_{bcb}^{(2)}$, and $\beta_{caa}^{(2)}=\beta_{cbb}^{(2)}$. When the relative angle between the two symmetrically stretching bonds in a C_{2v} symmetric molecule (e.g., the H–C–H angle in CH_2 or the H–O–H angle in water) is close to 109.5°, $\beta_{aac}^{(2)}$ approaches the value of $\beta_{ccc}^{(2)}$ (Refs. 3, 43, 44, and 49) so that β_1 vanishes. This is exactly the case for the CH_2 group that is present in, e.g., alkyl chains. For water, the angle is 104.5° so that a small β_1 of 0.07 remains.

TABLE II. Specific values for $\boldsymbol{\beta}^{(2)}$ for a water molecule and a CH_3 head group, for which $\beta_{aac}^{(2)}/\beta_{ccc}^{(2)}=3$. All values are scaled by an arbitrary factor so that either β_2 or β_3 is unity.

	SHS	SFS (ss)	SFS (as)
Water	$\beta_1=-2.69$ $\beta_2=\beta_3=1$ $\beta_4=0.69$	$\beta_1=0.07$ $\beta_2=1$	$\beta_1=-2$ $\beta_3=\beta_4=1$
CH_3		$\beta_1=-0.67$ $\beta_2=1$	$\beta_1=-2$ $\beta_3=\beta_4=1$

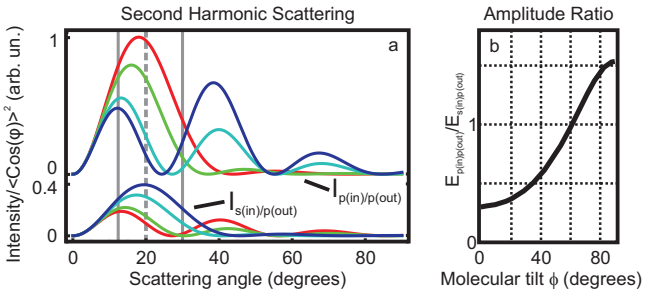

FIG. 3. (a) Variation in the angular SHS pattern as a function of molecular tilt angle ϕ in the case of water (C_{2v} symmetric). The scattering patterns for the p(in)p(out) and s(in)p(out) polarizations have been simulated for a particle radius of 500 nm and a fundamental wavelength of 800 nm. Since the source fields are degenerate, the opening angle $\beta=0$. The colored curves show the range of variation in the scattering pattern between 0° ($D=1$, red curves) and 90° ($D=0$, blue curves) molecular tilt, whereas the two gray curves represent the intermediate values of 30° and 60° molecular tilt ($D=0.75$ and $D=0.25$, respectively. For SHS from a 500 nm particle, the optimal angular range for orientation retrieval lies between 14° and 30° (gray lines). Since all expressions for scattered electric fields are linear combinations of $\boldsymbol{\chi}^{(2)}$ elements, and all of these elements contain a leading factor $\langle\cos\phi\rangle$, all intensities have been divided by the factor $\langle\cos\phi\rangle^2$ for ease of comparison. (b) Ratio of the electric field amplitude $E_{\mathrm{p(in)p(out)}}/E_{\mathrm{s(in)p(out)}}$ for a scattering angle of 20° [corresponding to the dashed vertical line in (a)]. At this scattering angle, the amplitude ratio increases for increasing molecular tilt.

III. RESULTS AND DISCUSSION

The magnitude of the second-order susceptibility and second-order polarization changes if the average molecular tilt angle changes. For a SHS or SFS experiment this means additionally that the angular distribution of the scattered second harmonic or sum frequency field might change. In this section we present simulations for a suspension of 500 nm radius particles consisting of centrosymmetric material. At the interface of these particles, inversion symmetry is broken.

A. Second harmonic scattering

For SHS, we have simulated scattering using a fundamental frequency of 800 nm wavelength. We show the scattering patterns of the p-polarized scattered light, either for a p-polarized [p(in)p(out)] or a s-polarized [s(in)p(out)] fundamental beam. We have chosen an interface covered with water molecules (C_{2v} symmetry), where we used $\boldsymbol{\beta}^{(2)}$ values from Zhang *et al.*,[48] who stated that $\beta_{ccc}^{(2)}$ can be neglected and who determined the ratio β_4/β_2 at 0.69 (see Table II). Figure 3 shows the variation in angular scattering pattern for these parameters. The colored curves show the range of variation in the scattering pattern for tilt angles between 0° ($D=1$, red curves) and 90° ($D=0$, blue curves). All electric fields are linear combinations of $\boldsymbol{\chi}^{(2)}$ so that the leading fac-

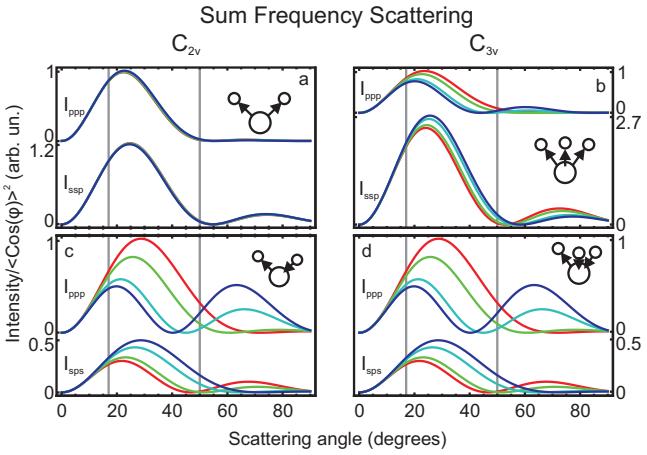

FIG. 4. Variation in the angular SFS pattern as a function of molecular tilt angle ϕ in the case of different vibrational modes: (a) water (C_{2v}) symmetric stretch, (b) CH_3 (C_{3v}) symmetric stretch, (c) water asymmetric stretch, and (d) CH_3 asymmetric stretch. Simulated are the vibrations of water (C_{2v}) and a CH_3 head group (C_{3v}), for the latter of which a ratio $\beta^{(2)}_{aac}/\beta^{(2)}_{ccc}$ of 3 has been arbitrarily set. The scattering patterns of the ppp and ssp (symmetric stretch) and ppp and sps (asymmetric stretch) polarization directions have been simulated for a particle radius of 500 nm and source beams of wavelengths 800 and 2666 nm (=3750 cm^{-1}, for water) or 3448 nm (=2900 cm^{-1}, for CH_3) with an opening angle of $\beta=15°$ ($\alpha=12°$). The red curves correspond to a molecular tilt angle of 0° ($D=1$), whereas the blue curves correspond to a tilt angle of 90° ($D=0$). The intermediate gray curves correspond to tilt angles of 30° ($D=0.75$) and 60° ($D=0.25$). The gray vertical lines indicate the range of scattering angles that is most sensitive to molecular orientation. For 500 nm particles, this range lies between 17° and 50°. Here also all intensities have been divided by the factor $\langle\cos\phi\rangle^2$ for ease of comparison.

tor $\langle\cos\phi\rangle$ in Eq. (13) becomes a leading factor in the expression for the electric field. Since this term does not influence polarization ratios, we have divided all intensities by a factor $\langle\cos\phi\rangle^2$ to maintain ease of comparison. A large variation in scattering pattern is observed due to the large value of $\beta_1=-2.69$. Figure 3(b) shows the ratio of the amplitudes of the two polarizations, $E_{p(in)p(out)}/E_{s(in)p(out)}$ as a function of molecular tilt. The ratio of $E_{p(in)p(out)}/E_{s(in)p(out)}$ yields a unique value for ϕ.

B. Sum frequency scattering

In the case of SFS, we consider two different types of surfaces: one consisting of C_{2v} symmetric molecules, where we again use the example of water, and one consisting of C_{3v} symmetric molecules, e.g., methyl groups. Table II summarizes the values for $\boldsymbol{\beta}^{(2)}$ used for the symmetric and asymmetric stretch vibrations of both molecules. Values for $\boldsymbol{\beta}^{(2)}$ were taken from Gan *et al.*[49] for the water molecules ($\beta_1=0.07$, $\beta_2=1$ for the ss, and $\beta_1=-2$ and $\beta_3=\beta_4=1$ for the as). For the vibrations of the CH_3 head group, the determining parameter is the ratio $\beta^{(2)}_{aac}/\beta^{(2)}_{ccc}$, which typically ranges between[3] 1.6 and 4. For this simulation, we have arbitrarily set this value to 3 so that $\beta_1=-0.67$ and $\beta_2=1$. The asymmetric stretch vibration does not depend on this parameter so that the values for $\boldsymbol{\beta}^{(2)}$ are identical to those of water. Figure 4 shows the variation in angular scattering pattern for different vibrational modes: (a) water (C_{2v}) symmetric stretch, (b) CH_3(C_{3v}) symmetric stretch, (c) water asymmetric stretch, and (d) CH_3 asymmetric stretch. Shown are the intensities of the ppp [(a)–(d)], ssp [(a) and (c)], and sps [(b) and (d)] polarizations as a function of scattering angle for an experiment in which a visible laser pulse of 800 nm and infrared laser pulse at the resonance frequency of the vibration (2666 nm=3750 cm^{-1} for water and 3448 nm =2900 cm^{-1} for CH_3) are overlapped with an angle of 15° with respect to each other. Again, the colored curves show the range over which the scattering pattern varies when the average molecular tilt varies from 0° ($D=1$, red curve) to 90° ($D=0$, blue line).

In the case of the water symmetric stretch resonance, variations as a result of molecular tilt are minimal, which makes this resonance unfavorable for orientational analysis. This insensitivity is an intrinsic property of the molecule:[49] The value of β_1 is close to 0 (for water, $\beta_1=0.07$). Since the orientation parameter D exclusively couples to β_1 [see Eq. (13)], a vanishing β_1 results in an expression for $\boldsymbol{\chi}^{(2)}$ that is insensitive to the molecular orientation. The same holds true for any molecular vibration with vanishing β_1, e.g., the symmetric stretch of methylene (CH_2). For the C_{3v} symmetric methyl stretch, however, β_1 differs from 0 ($\beta_1=-0.67$). The angular scattering pattern is therefore sensitive to molecular orientation. The same holds for the asymmetric stretch vibration for both symmetries. The angular scattering patterns each depend only on β_3 and are identical. Since $\beta_1=-2\beta_3$ significantly differs from zero, the largest variation as a function of orientation is observed for this vibration.

It is possible to extract molecular orientation from the variations in scattering intensity between polarizations. Figures 5(a) and 5(b) show the SFS signal amplitude at different polarizations relative to that of the ppp polarization, as a function of the average tilt angle ϕ of the molecular group. Shown are the ratios for the symmetric (dashed curves) and asymmetric (solid curves) vibrations for water molecules [Fig. 5(a)] and CH_3 head groups [Fig. 5(b)]. These values have been calculated at a scattering angle of 33° ($qR=2.7$). Although the amplitude ratios for the symmetric stretch vibrations are insensitive to ϕ, the ratios for the asymmetric stretch vibrations can be used to extract orientation. Calculating the ratio E_{sps}/E_{ppp}, for instance, uniquely establishes a value for ϕ.

Another useful way of obtaining information about the molecular tilt angle is to explore the signal strength between two perpendicular modes of the same moiety.[3,50] The relative strength of a symmetric and asymmetric resonance is determined by the relative value of $\boldsymbol{\beta}^{(2)}$ components, e.g., β_2 and β_4. Because these are molecular properties, it is also possible to gain information on molecular orientation by comparing the relative strength of the symmetric and asymmetric resonance peaks. Figures 5(c) and 5(d) show the ratios of the amplitudes of the symmetric and asymmetric stretch modes as a function of average molecular orientation for the same parameters as Fig. 4. These ratios depend on the relative values of β_2 and β_4, and are therefore expressed in units of β_2/β_4. It is clear that, for instance, in the ppp polarization the symmetric stretch mode dominates when molecular orientation is nearly perpendicular to the interface ($\phi=0$), while for large tilt angles the asymmetric stretch signal should be

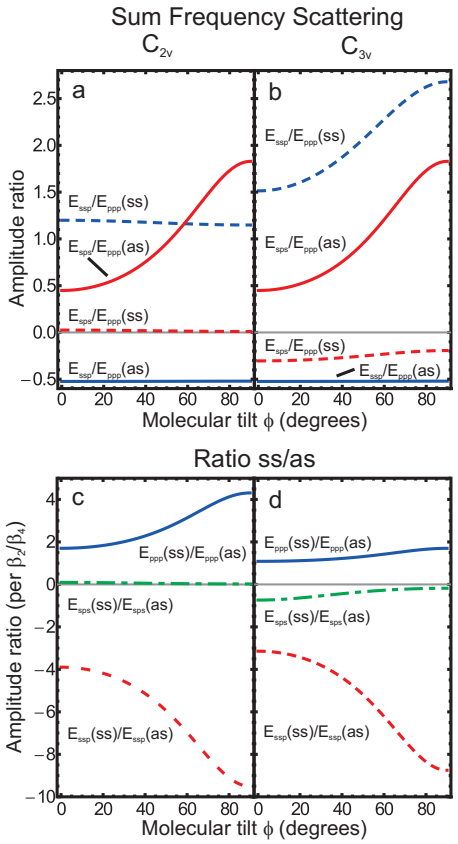

FIG. 5. Electric field amplitude ratios as a function of molecular tilt, for the same parameters as in Fig. 4. All amplitude ratios were simulated at $qR=2.7$ [equivalent to a scattering angle of 33° in Figs. 4(c) and 4(d)]. (a) Ratio of E_{ssp}/E_{ppp} (blue curves) and E_{sps}/E_{ppp} (red curves) for the ss (dashed curves) and as (solid curves) vibrations of water (C_{2v} symmetry). (b) Idem, but for a CH_3 group (C_{3v} symmetry). For both water and CH_3, the as mode mostly contributes to the ppp, sps, and pss (not shown) polarizations. From the ratio between ppp and sps or pss, the average molecular tilt can be extracted. [(c) and (d)] Ratios between the ss and as vibrations of (c) water and (d) CH_3 for ppp (solid curve), ssp (dashed curve), and sps (dashed-dotted curve). Ratios between ss and as modes are expressed in multiples of the value of β_2/β_4.

stronger. When the values of $\beta^{(2)}_{caa}$, $\beta^{(2)}_{cbb}$, and $\beta^{(2)}_{ccc}$ are known, it is possible to extract molecular orientation from a single spectral measurement at a fixed polarization combination. Even when the values of the $\boldsymbol{\beta}^{(2)}$ tensor are not known *a priori*, the ss/as ratio still serves as an indicator for relative orientation and may be employed to track changes in orientation, or the absence thereof.

C. Angular dependence

Figures 4 and 3 both show that at low scattering angles, intensity variations are minimal. Only at angles above 14° (SHS) or 17° (SFS), which both correspond to $qR>1.4$, these intensity variations increase. At higher angles, the scattered intensity is sensitive to molecular orientation. Increasing the scattering angle further, however, reduces the overall signal strength and therefore the signal-to-noise ratio. Thus, the optimal angular range for orientational analysis is the interval between 14° and 30° in the case of SHS or between 17° and 50°, in the case of SFS, which in both cases corresponds to $1.4<qR<4$. For particles of sizes other than 500 nm, the optimal angular range can be derived from the relation $qR=2k_0R\sin(\theta/2)$. Figure 6 shows the optimal scattering angles for particles of a size other than 500 nm, both for SFS (hatched area) and for SHS (gray area). As the particle size decreases, the optimal angular range moves to higher angles.

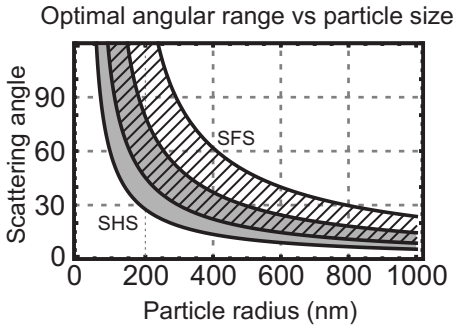

FIG. 6. Angular position of the optimal interval of $qR=1.4-4$ for a evanescent wavelength of 645 nm (hatched area) and 400 nm (gray area). The lower and upper curves each correspond to the boundaries of $qR=1.4$ and $qR=4$, respectively. The curves show that the lower the particle radius, the higher a scattering angle must be chosen to determine molecular orientation. Moreover, it is shown that the optimum range for SHS lies at lower angles than that for SFS.

IV. CONCLUSION

We have described how molecular orientation can be determined from SHS and SFS experiments. The dependence of the effective susceptibility on the scattering angle leads to an optimal angular range at which orientation measurements are most sensitive. For the asymmetric stretch mode of a C_{2v} or C_{3v} point group, this is the range from $qR=1.4$ to $qR=4$. Established methods, such as analyzing the polarization intensity ratio,[3,51] the polarization null method[3,8,52,53] or analyzing the resonance amplitude ratio[3,50] can be applied. Moreover, the angular scattering pattern of nonlinear light scattering experiment adds another dimension of information, which allows for a more accurate fit to a theoretical curve. Finally, we have made a simulation program for the angular scattering pattern available at http://www.mf.mpg.de/en/abteilungen/roke/simulation.html.

ACKNOWLEDGMENTS

This work is part of the research program of the Max Planck Society. Additional funding was received from the German Science Foundation (DFG) under Contract No. 560398 and the European Research Council (ERC) under Contract No. 240556.

[1] T. F. Heinz, *Nonlinear Surface Electromagnetic Phenomena* (Elsevier, New York, 1991) Chap. 5, p. 353.
[2] Y. R. Shen, Nature (London) **337**, 519 (1989).
[3] H. F. Wang, W. Gan, R. Lu, Y. Rao, and B. H. Wu, Int. Rev. Phys. Chem. **24**, 191 (2005).
[4] A. J. Moad and G. J. Simpson, J. Phys. Chem. B **108**, 3548 (2004).
[5] C. A. Dailey, B. J. Burke, and G. J. Simpson, Chem. Phys. Lett. **390**, 8 (2004).
[6] W. K. Zhang, H. F. Wang, and D. S. Zheng, Phys. Chem. Chem. Phys. **8**, 4041 (2006).
[7] C. Hirose, H. Yamamoto, N. Akamatsu, and K. Domen, J. Phys. Chem. **97**, 10064 (1993).
[8] R. Lu, W. Gan, B. H. Wu, H. Chen, and H. F. Wang, J. Phys. Chem. B

108, 7297 (2004).
[9] R. Lu, W. Gan, B. H. Wu, Z. Zhang, Y. Guo, and H. F. Wang, J. Phys. Chem. B **109**, 14118 (2005).
[10] Q. Du, R. Superfine, E. Freysz, and Y. R. Shen, Phys. Rev. Lett. **70**, 2313 (1993).
[11] H. Chen, W. Gan, B. H. Wu, D. Wu, Y. Guo, and H. F. Wang, J. Phys. Chem. B **109**, 8053 (2005).
[12] H. Chen, W. Gan, B. H. Wu, D. Wu, Z. Zhang, and H. F. Wang, Chem. Phys. Lett. **408**, 284 (2005).
[13] X. Zhuang, P. B. Miranda, D. Kim, and Y. R. Shen, Phys. Rev. B **59**, 12632 (1999).
[14] Note that in this manuscript, we denote the molecular tilt angle with "ϕ" rather than the more commonly used "θ" since θ is reserved for the scattering angle.
[15] H. Wang, E. C. Y. Yan, E. Borguet, and K. B. Eisenthal, Chem. Phys. Lett. **259**, 15 (1996).
[16] E. C. Y. Yan, Y. Liu, and K. B. Eisenthal, J. Phys. Chem. B **102**, 6331 (1998).
[17] H. F. Wang, E. C. Y. Yan, Y. Liu, and K. B. Eisenthal, J. Phys. Chem. B **102**, 4446 (1998).
[18] L. Schneider, H. J. Schmid, and W. Peukert, Appl. Phys. B: Lasers Opt. **87**, 333 (2007).
[19] N. Yang, W. E. Angerer, and A. G. Yodh, Phys. Rev. Lett. **87**, 103902 (2001).
[20] E. C. Y. Yan and K. B. Eisenthal, J. Phys. Chem. B **103**, 6056 (1999).
[21] E. C. Y. Yan and K. B. Eisenthal, Biophys. J. **79**, 898 (2000).
[22] Y. Jiang, P. T. Wilson, M. C. Downer, C. W. White, and S. P. Withrow, Appl. Phys. Lett. **78**, 766 (2001).
[23] K. B. Eisenthal, Chem. Rev. (Washington, D.C.) **106**, 1462 (2006).
[24] S. H. Jen and H. L. Dai, J. Phys. Chem. B **110**, 23000 (2006).
[25] R. K. Campen, D. S. Zheng, H. F. Wang, and E. Borguet, J. Phys. Chem. C **111**, 8805 (2007).
[26] H. F. Wang, T. Troxler, A. G. Yeh, and H. L. Dai, J. Phys. Chem. C **111**, 8708 (2007).
[27] S. H. Jen, G. Gonella, and H. L. Dai, J. Phys. Chem. A **113**, 4758 (2009).
[28] S.-H. Jen, H.-L. Dai, and G. Gonella, J. Phys. Chem. C **114**, 4302 (2010).
[29] S. Roke, W. G. Roeterdink, J. E. G. J. Wijnhoven, A. V. Petukhov, A. W. Kleyn, and M. Bonn, Phys. Rev. Lett. **91**, 258302 (2003).
[30] S. Roke, J. Buitenhuis, J. C. van Miltenburg, M. Bonn, and A. van Blaaderen, J. Phys.: Condens. Matter **17**, S3469 (2005).
[31] S. Roke, O. Berg, J. Buitenhuis, A. van Blaaderen, and M. Bonn, Proc. Natl. Acad. Sci. U.S.A. **103**, 13310 (2006).
[32] A. G. F. de Beer, H. B. de Aguiar, J. W. F. Nijsen, and S. Roke, Phys. Rev. Lett. **102**, 095502 (2009).
[33] S. Roke, ChemPhysChem **10**, 1380 (2009).
[34] H. B. de Aguiar, A. G. F. de Beer, M. L. Strader, and S. Roke, J. Am. Chem. Soc. **132**, 2122 (2010).
[35] J. Martorell, R. Vilaseca, and R. Corbalan, Phys. Rev. A **55**, 4520 (1997).
[36] J. I. Dadap, J. Shan, K. B. Eisenthal, and T. F. Heinz, Phys. Rev. Lett. **83**, 4045 (1999).
[37] S. Roke, M. Bonn, and A. V. Petukhov, Phys. Rev. B **70**, 115106 (2004).
[38] J. I. Dadap, J. Shan, and T. F. Heinz, J. Opt. Soc. Am. B **21**, 1328 (2004).
[39] A. G. F. de Beer and S. Roke, Phys. Rev. B **75**, 245438 (2007).
[40] J. I. Dadap, Phys. Rev. B **78**, 205322 (2008).
[41] A. G. F. de Beer and S. Roke, Phys. Rev. B **79**, 155420 (2009).
[42] J. I. Dadap, H. B. de Aguiar, and S. Roke, J. Chem. Phys. **130**, 214710 (2009).
[43] C. Hirose, N. Akamatsu, and K. Domen, J. Chem. Phys. **96**, 997 (1992).
[44] C. Hirose, N. Akamatsu, and K. Domen, Appl. Spec. **46**, 1051 (1992).
[45] G. J. Simpson and K. L. Rowlen, J. Am. Chem. Soc. **121**, 2635 (1999).
[46] S. H. Lee, J. Wang, S. Krimm, and Z. Chen, J. Phys. Chem. A **110**, 7035 (2006).
[47] V. Ostroverkhov, K. D. Singer, and R. G. Petschek, J. Opt. Soc. Am. B **18**, 1858 (2001).
[48] W. K. Zhang, D. S. Zheng, Y. Y. Xu, H. T. Bian, Y. Guo, and H. F. Wang, J. Chem. Phys. **123**, 224713 (2005).
[49] W. Gan, D. Wu, Z. Zhang, R. R. Feng, and H. F. Wang, J. Chem. Phys. **124**, 114705 (2006).
[50] G. Ma and H. C. Allen, Langmuir **22**, 11267 (2006).
[51] M. J. Shultz, C. Schnitzer, D. Simonelli, and S. Baldelli, Int. Rev. Phys. Chem. **19**, 123 (2000).
[52] Y. Rao, Y. S. Tao, and H. F. Wang, J. Chem. Phys. **119**, 5226 (2003).
[53] R. Lu, W. Gan, and H. F. Wang, Chin. Sci. Bull. **48**, 2183 (2003).